ROYAL SOCIETY OF CHEMISTRY

PAPER

Check for updates

An improved protocol for LA-MC-ICP-MS isotope ratio measurements of natural silicon at 213 nm: comparison of mass bias correction factor dependence (solution *vs.* solid single crystal) and solid sample homogeneity†

Tongxiang Ren, [ID] [a] Olaf Rienitz, [ID] [b] Tianheng Gao [ID] [a] and Axel Pramann [ID] *[b]

Nanosecond scanning laser ablation MC-ICP-MS (213 nm) was applied to the measurement of the intensity ratios of ultrapure single crystalline silicon (WASO04), which is used in the XRCD-method and general silicon isotope ratio measurements as a well characterized reference material. Parallel measurements in the same sequence with WASO04 samples (w(Si) = 4 µg g^{-1}) dissolved in TMAH (w(TMAH) = 0.0006 g g^{-1}) were conducted for the comparison of matrix and experimental related impact parameters of the derived calibration factors (K) for the correction of intensity ratios. Uncertainties associated with K factors determined *via* solid laser ablation multicollector-inductively coupled plasma mass spectrometry (LA-MC-ICP-MS) were in the range of $u_{rel}(K(^{29}Si/^{28}Si))$ = 0.58%, $u_{rel}(K(^{30}Si/^{28}Si))$ = 0.60%, and $u_{rel}(K(^{30}Si/^{29}Si))$ = 0.47%, and exhibit a scattering contribution of up to 50%, whereas K factors derived by Si samples in solution under the same conditions show a more stable course. Main influences on isotope fractionation were derived from the applied laser parameters. Matrix influences due to the kind of sample (solid or dissolved) are negligible. A "quasi-homogeneity" investigation of the local distributions of amount-of-substance fractions $x(^{i}Si)$ in the solid sample shows a uniform distribution within the limits of uncertainties. A measurement protocol of isotope ratios of natural silicon was developed using scanning LA-MC-ICP-MS, applying 10^{13} Ω resistors for Faraday detector readings of highest sensitivity, τ-correction, measurements of interference free (high resolution) Si signals, and strong depletion of the NO$^+$ interference near the ^{30}Si$^+$ signal.

1. Introduction

The production and application of silicon crystals in semi-conductors and micro-electronics materials are increasing not only in industry and economics, but also in analytical sciences, ensuring the purity and quality of the respective materials.[1,2] In basic metrology, single crystalline silicon has become a material of major interest in the last decades since it was used as the key material in the redetermination of the Avogadro constant N_A, and later on for the redefinition of the SI units, the mole and the kilogram, when applying the X-ray crystal density (XRCD) method acting as the underlying primary method.[3–5] Prior to the use of silicon highly enriched in the ^{28}Si isotope, high purity single crystalline silicon with approximately natural isotopic

composition with amount-of-substance fractions $x(^{28}Si)$ ≈ 0.922 mol mol^{-1}, $x(^{29}Si)$ ≈ 0.047 mol mol^{-1}, and $x(^{30}Si)$ ≈ 0.031 mol mol^{-1} has been used for the XRCD experiments.[6] The two main Si crystal materials with this background used were the so-called NRLM4 crystal (name defined by the former National Research Laboratory of Metrology, Japan) from the National Metrology Institute of Japan (NMIJ) and the WASO04 crystal (name defined by the "Wacker-Siltronic" company, Germany) from the Physikalisch-Technische Bundesanstalt (PTB) in Germany.[6–9] These crystals have been completely characterized at that time for a first attempt of an estimate of N_A with the lowest associated uncertainty. Although the use of natural-like Si crystal yields a lower limit of $u_{rel}(N_A)$ = 3.1 × 10^{-7}, which was at least one order of magnitude too high to become a candidate material for a redetermination, the WASO04 crystal material today still plays a prominent role in the determination of the molar mass and isotopic composition of the new silicon crystals highly enriched in ^{28}Si, which enables the determination of $u_{rel}(N_A)$ < 1 × 10^{-8} – a prerequisite for the revision of the kilogram and mole in 2019 and further dissemination of these SI units today and in the future.[9,10] The respective molar mass

[a] Division of Chemical Metrology and Analytical Science, National Institute of Metrology, Beijing 100029, China

[b] Physikalisch-Technische Bundesanstalt (PTB), Bundesallee 100, 38116 Braunschweig, Germany. E-mail: axel.pramann@ptb.de

This journal is © The Royal Society of Chemistry 2025

J. Anal. At. Spectrom., 2025, **40**, 1323–1334 | 1323

determinations were performed by isotope ratio mass spectrometry using the virtual-element isotope dilution mass spectrometry method.[11] This method requires for the correction of isotope ratios in the sample and blends a material with known isotope ratios.[12] For this purpose, WASO04 was isotopically characterized using an FGIM approach.[12,13] This way it became the necessary material with known absolute isotope ratios and is still used as a reference material in case of silicon isotope ratio measurements and molar mass determinations of Si highly enriched in ^{28}Si or for calibration in Instrumental Neutron Activation Analysis (INAA).[9] In 2019, PTB reported on the use of three classes of silicon sphere standards ("artefacts") for the realization and distribution of the kilogram, which can be used for different levels of uncertainty in the dissemination chain: from metrology to industrial application.[14] The three Si sphere types are: "^{28}Si-primary" (Si crystal highly enriched in ^{28}Si, with $u_{rel}(m) \approx 2 \times 10^{-8}$); "^{nat}Si-quasi primary" (Si crystal with natural isotopic composition, with $u_{rel}(m) \approx 3 \times 10^{-8}$) and "^{nat}Si-secondary" (industrially manufactured Si crystal with natural isotopic composition, with $u_{rel}(m) \geq 3 \times 10^{-8}$). To consider both availability and production costs, the two latter sphere materials are machined from natural silicon. This material can even be calibrated and characterized according to its isotopic composition with the reference material WASO04 in the future.

Si isotope ratio measurements with the lowest associated uncertainties are best carried out by isotope ratio mass spectrometry using inductively coupled plasma source (ICP-MS) instruments.[15] However, solutions are usually necessary for ICP-MS measurements, which is connected to a time-consuming and complex sample preparation procedure, and with the advantage of achieving intensity ratios with relative uncertainties in the 10^{-5} range. An alternative sample introduction is laser ablation ICP-MS (LA-ICP-MS), a versatile analytical tool established in recent decades.[16,17] Since the pioneering work of Gray in 1985, numerous applications and publications have been developed and published, so LA-ICP-MS is now a common tool in geosciences, forensics, biology, related interdisciplinary fields, and analytical chemistry.[18] Its main advantages are saving time in sample preparation and the ability to scan local variations of sample contents or isotope ratios in a highly spatially resolved mode down to a few micrometer, as well as depth profiling. Therefore, mapping structures and compositions of tiny samples is possible, and furthermore, LA-ICP-MS enables a somewhat non-destructive or "minimally invasive" analysis of rare samples.

In the current study, we applied for the first time LA-MC-ICP-MS isotope ratio measurements on an ultrapure single crystalline silicon material used in the XRCD method as a reference material for K factor determinations in the context of the measurement of the isotopic composition and molar mass of silicon highly enriched in ^{28}Si. The isotope ratios of this Si material (WASO04) have been well characterized and determined using a gravimetric mixture approach.[10,11] This study's main objective is to compare the K factors determined using a pure solid crystal sample *via* LA-MC-ICP-MS with the respective K factors obtained by measuring a Si sample in the solution

under the same conditions.[19,20] The range of isotope fractionation and underlying matrix effects were probed. In this context, a stable protocol for scanning LA-MC-ICP-MS was developed using high ohmic 10^{13} Ω resistors in the feedback loop of the Faraday cups for the highest sensitivity which enables measurements of small ion beams ($U \leq 5$ mV corresponding to 3×10^5 s^{-1} (counts per second)), *e.g.*, in the case of Si highly enriched in ^{28}Si.[21,22] Influences of crucial parameters such as scanning speed, spot size, laser energy, and laser frequency were investigated. Additionally, a rough "quasi-homogeneity" investigation of the solid sample used was performed, comparing the amount-of-substance fractions $x(^iSi)$ of all three Si isotopes (i) averaged from the respective line scan areas. Data evaluation and uncertainty calculations were carried out using the rules of the "Guide to the Expression of Uncertainty in Measurement" (GUM).[23]

2. Experimental
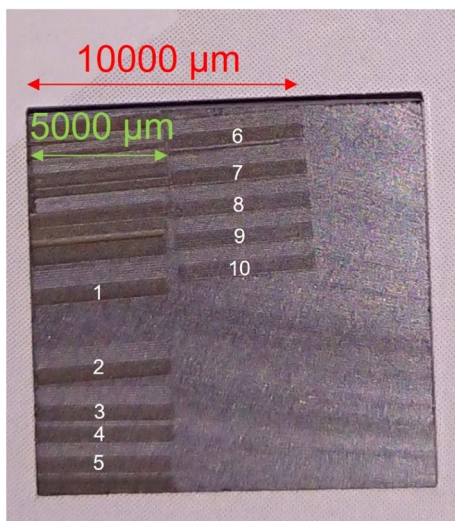
2.1 Materials and reagents

The basic sample material is single crystalline silicon (WASO04), highly purified and produced by float zone melting by the company Wacker-Siltronic, Germany, in collaboration with PTB about 20 years ago in the context of the redetermination of the Avogadro-constant.[6–9] This material is well characterized and was used in the XRCD method to measure the isotopic composition and molar mass of silicon crystals highly enriched in ^{28}Si.[10] Various mass spectrometric measurements applied during the last years used the WASO04 Si with an almost natural isotopic composition for the fractionation correction (mass bias), especially for the correction of the intensity ratios $r(U(^{30}Si)/U(^{29}Si))$ in the respective samples.[24] Detailed descriptions of the sample preparation and related procedures can be found elsewhere.[10] The respective bottles and vials are made of PFA (perfluoroalkoxy alkane) and were cleaned according to a special protocol.[10] In brief, for the solution measurements, approximately 50 mg of the WASO04 crystal material (cleaned and surface-etched) have been dissolved in aqueous tetramethylammonium hydroxide (TMAH, $w = 0.25$ g g^{-1}, Alfa Aesar, Thermo Fisher GmbH, Kandel, Germany with electronic grade purity 99.9999%).

After further dilution using purified water (Merck Millipore™ water purification system yielding 18 MΩ cm resistivity), measurement solutions with $w(Si) = 4$ μg g^{-1} in aqueous TMAH with $w(TMAH) = 0.0006$ g g^{-1} have been prepared. The liquid blank also consists of TMAH$_{aq}$ with $w(TMAH) = 0.0006$ g g^{-1}. For laser ablation measurements, a solid single crystal sample (WASO04) of quadratic shape (edge length ≈ 15 mm, thickness ≈ 3 mm) with a polished and cleaned surface was used (see Fig. 1).

2.2 Mass spectrometry

The mass spectrometric measurements were carried out at PTB using a high-resolution multicollector-inductively coupled plasma mass spectrometer (MC-ICP-MS) Neptune™ XT (Thermo Fisher Scientific GmbH, Bremen, Germany).[22,24] All

1324 | *J. Anal. At. Spectrom.*, 2025, **40**, 1323–1334

This journal is © The Royal Society of Chemistry 2025

Fig. 1 Photograph of a WASO04 Si sample (natural isotopic composition) after laser ablation scans using $\lambda = 213$ nm. The rectangular sample consists of a purified single crystal with approximately 15 mm × 15 mm. Lengths of ablation scan lines were approximately 5000 μm. Numbers indicate the line scans and corresponding sequences used for isotope ratio measurements.

Table 1 Neptune XT™ MC-ICP-MS operation parameters

Vacuum	Scroll pump, turbo pumps, OnToolBooster pump
Sample introduction system	PFA nebulizer (50 μL min^{-1}), cyclonic spray chamber (PEEK) and Y-piece (PTFE), sapphire torch and injector, BN bonnet, X-skimmer and sampler cone (both Ni)
Flow rates (Argon 5.0)	Cool gas: 16 L min^{-1}, auxiliary gas: 0.8 L min^{-1} Sample gas: 0.8–1.0 L min^{-1}
Machine settings	Pseudo high resolution HR ($M/\Delta M = 8000$) Plasma power $P(\text{RF}) = 1200$ W
Autosampler	CETAC ASX 110 FR
Sequence settings	Wash time: 60 s Take-up time: 30 s
Blank measurement	LA: gas blank, dissolved sample: TMAH blank
Faraday detectors, resistors	L3: $^{28}\text{Si}^+$ (10^{11} Ω); C: $^{29}\text{Si}^+$ (10^{13} Ω), H3: $^{30}\text{Si}^+$ (10^{13} Ω)
Integration time/s	2.1
Idle time/s	3
Number of integrations	1
Number of cycles/block	60
Number of blocks	1

measurements were performed using a combination of 10^{11} Ω amplifiers (Faraday cup L3, $^{28}\text{Si}^+$) and 10^{13} Ω amplifiers (Faraday cups C ($^{29}\text{Si}^+$) and H3 ($^{30}\text{Si}^+$)). High-ohmic resistors applied for the detection of the two lower abundant Si isotopes were tested in combination with LA signal accumulation and sensitivity increase.

An additional contribution to biased isotope ratios can occur due to signal detection of Faraday collectors, especially in the case of transient laser signals when using high ohmic resistors in the feedback loop of the respective amplifiers. Different signal decay times correspond to so-called "first-order-tau-constants" of the respective resistor.[22,25,26] To minimize influences inducing a related bias in isotope ratios, the generated data were corrected by the tau constants (τ) of the respective amplifiers implemented in the Neptune XT software. The potential effect of τ-corrections has been investigated elsewhere.[22]

Table 1 summarizes the applied experimental parameters and operation conditions.

The sample introduction consists of a home-built Y-piece made of PTFE for mixing the laser ablation and dissolved sample aerosols and a cyclonic spray chamber made of PEEK (solution sample arm).[27] The ICP torch is made mainly of sapphire parts. In the case of the dissolved sample, tentative contaminations were corrected by subtracting the blank signals measured prior to the sample from the latter, whereas, in the case of the laser ablation, a gas blank was subtracted from the sample signals. The plasma generated by the laser ablation was transferred via pure He (5.0, Linde, Germany) through a tube ("SQUID", made of PEEK and nylon tubing, Laurin Technic, Australia) intended as a signal smoothing device. During the LA measurements, DI water aerosol was transferred through the

solution arm of the Y-piece to reduce any nitrogen addition (reduction of NO^+ interferences on mass $m/z \approx 30$) to the plasma.[28]

Laser ablation was carried out using a commercially available ESI 213 NWR (Elemental Scientific Lasers, USA) system with a pulsed 213 nm Nd:YAG laser; see Table 2. The laser was used to trigger the MS-experiment (sequence). In this study, line scans were performed to guarantee proper timing of the laser pattern connected to a sequence, including measurements of a dissolved sample. Additionally, the scanning mode enables signal stabilization after an appropriate choice of parameters (scan speed and spot size). Line scans also have the advantage of yielding an average composition of the sample used (larger

Table 2 Typical laser parameters

Type	ESI NWR 213, solid state Nd:YAG
Wavelength/nm	213
Output energy/%	50
Pulse duration/ns	4
Sampling mode	Line scan (5000 μm)
Repetition rate/Hz	20
Spot size (diam.)/μm	20
Scan speed/μm s^{-1}	35
He gas flow rate/mL min^{-1}	450
Aerosol transport	SQUID-tubing
Ablation chamber	Two-volume chamber with reduced outer volume
Preablation	Output energy: 10%; spot size: 40 μm; scan speed: 55 μm s^{-1}, rep. rate: 20 Hz
Signal trigger	Sync out (trigger for MC-ICP-MS sequence)

This journal is © The Royal Society of Chemistry 2025

J. Anal. At. Spectrom., 2025, **40**, 1323–1334 | 1325

area) if an average value of the measured parameters (*e.g.*, intensity ratios of a reference material) will be used for related single samples.[29] In this study, we compared the averaged

results of different line scans on different sample locations, which is addressed as "quasi-homogeneity" due to the larger area instead of spot measurements, which were used for more
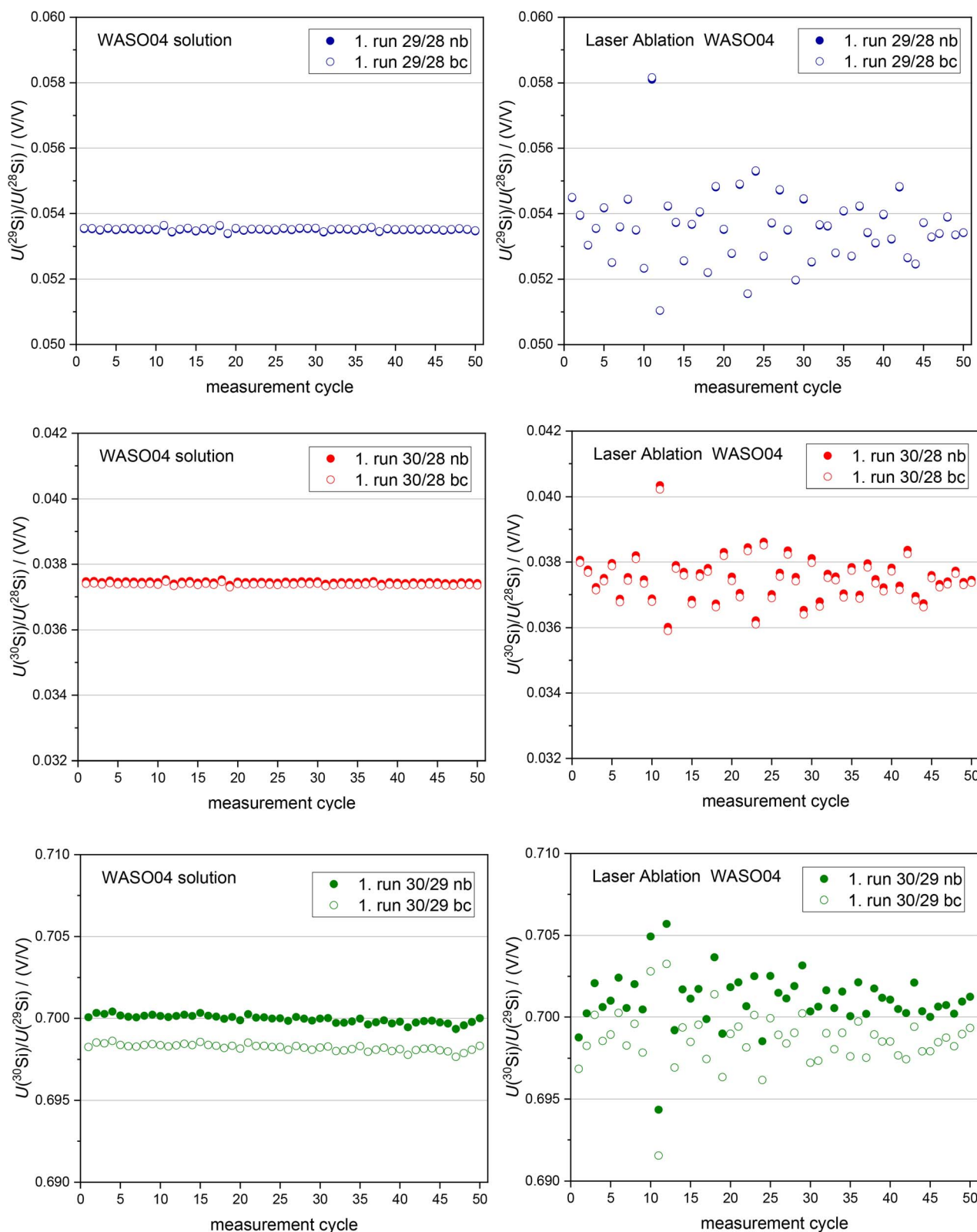
Fig. 2 Signal intensity ratios $r = U(^{i}\mathrm{Si})/U(^{j}\mathrm{Si})$ of the sample in solution compared with the solid sample (LA). Displayed is one run of each sample in a representative sequence (no. 6), demonstrating offsets between blank corrected and not blank corrected signals.
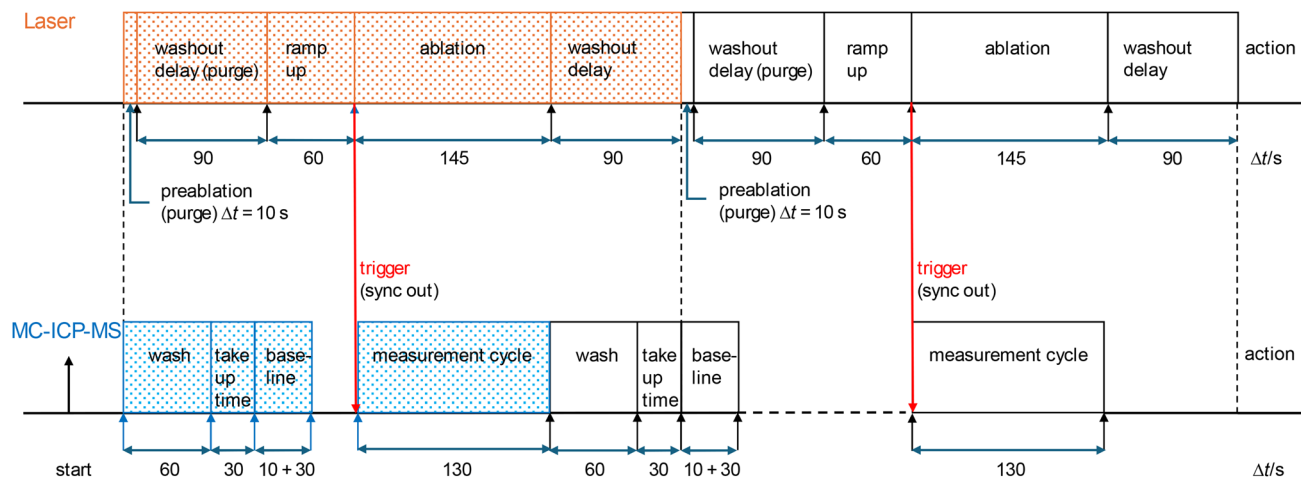
1326 | *J. Anal. At. Spectrom.*, 2025, **40**, 1323–1334

This journal is © The Royal Society of Chemistry 2025

Fig. 3 Schematic of the timing of the combination of the laser pattern and the MC-ICP-MS sequence. Prior to the ablation, the laser triggers the data collection (measurement) of the MC-ICP-MS (see text).

locally focused homogeneity studies in the range of 10–100 μm diameters.

Typical signal intensities were as follows: dissolved sample: $U(^{28}Si) \approx 4.8$ V, $U(^{29}Si) \approx 260$ mV, $U(^{30}Si) \approx 180$ mV; LA: $U(^{28}Si) \approx 5.5$ V, $U(^{29}Si) \approx 290$ mV, $U(^{30}Si) \approx 200$ mV.

A sequence consists of 14 runs (methods): one gas-blank, six LA solid Si sample measurements, six solution Si sample measurements, and one final (TMAH) blank measurement for solution correction. Fig. 2 displays the courses of measured intensity ratios r of sequence 6 exemplified: in the WASO04 solutions and in the LA process, a drastically different scattering of the ratios can be observed. Each plot displays one cycle of a sequence. The respective plots of solutions show that blank correction is necessary: see $U(^{30}Si)/U(^{28}Si)$ and $U(^{30}Si)/U(^{29}Si)$.

The observation of increased scattering of the course of intensity ratios when applying laser ablation can be also explained by a kind of a "melting effect" due to the use of a ns systems which releases the heat of the laser spot on the surface within a longer time period compared to a femtosecond ablation system.[20]

To avoid any carry-over effects and contamination, a sufficient wash time was applied. For solution measurements and LA the same method (and cup configuration) was used. Fig. 3 schematically displays the time scale (time intervals Δt) and respective – coincident – actions from the laser and the MC-ICP-MS. According to the applied parameters (*e.g.* wash time, laser parameters *e.g.* scan speed *etc.*), the time settings between the laser and the MC-ICP-MS sequence have to be aligned. The optimized protocol, including LA line scans and solution sample measurements, is based on the trigger signal (sync out) initiated by the laser system. In Fig. 3 the upper (orange-coloured) time scale shows the laser actions (preablation, washout delay, He gas ramp up delays, sample ablation…) connected with the actions of the MC-ICP-MS (sequence) shown in the lower (blue-coloured) time scale. It is important that, *e.g.*, the washout delay and ramp up time of the laser pattern includes the next wash time, take up time, and baseline measurement of the sequence; then data sampling in the

sequence starts after the next trigger signal of the laser. During the measurements of the dissolved sample and the blanks, the laser output energy was set to 0%.

All data generated were further evaluated independently of any instrumental software. Due to signal delay and strong scattering, the data of the first ten cycles of each block were rejected.

3. Results and discussion

3.1 Optimization of measurement protocol combining dissolved and solid samples

One task of this study was the development of an improved measurement protocol for the measurement of solvated and solid samples in a combined single sequence. In the case of the blank and sample in solution, standard optimization of the MC-ICP-MS parameters is sufficient, yielding high signal stability throughout all measurements. However, laser ablation measurements have to be optimized with respect to a number of parameters to match signal intensities and signal fluctuations.[30–32]

In the current measurements, the high mass resolution (HR) mode was applied to be as sure as possible to be free of any mass interferences near the Si isotope under investigation. After warming up, mass scans around the respective Si isotopes were performed prior to the measurements for both dissolved and solid samples. Respective mass scans are given in the ESI 1† (tuning). There, the traces of mass scans of WASO04 are plotted together on the axis of the $m/z = 29$ range.

No interferences were observed at the desired mass in static measurements. Using natural Si samples, especially the $^{28}Si^1H$ interference is not present (only when using enriched Si samples – which was not performed here). For the ^{29}Si trace, the $^{14}N_2{}^1H$ interference, and for ^{30}Si the $^{14}N^{16}O$ interference can be observed. The strong scattered signals of the LA traces compared to scans in the liquid resulted from intensity fluctuation and limited point resolution of scan steps. During a multicollector measurement however, a certain fixed mass is

This journal is © The Royal Society of Chemistry 2025

J. Anal. At. Spectrom., 2025, **40**, 1323–1334 | **1327**

measured yielding accumulated signals (and ratios) of a longer time period of comparable quality as in the liquid samples.

The application of 10^{13} Ω resistors for the detection of the lower abundant ^{29}Si and ^{30}Si signals in this study was chosen to enable a general detection of smaller intensities. This will allow a reduction of laser energy and still sufficient intensity of the latter isotopes. The main intention however, is a tentative capability of the detection of strongly depleted ^{29}Si and ^{30}Si signals, when measuring Si samples highly enriched in ^{28}Si. This has been conducted and discussed in a previous study using dissolved highly enriched samples.[22] A quantitative comparison of the influence of using mixed (10^{11} Ω and 10^{13} Ω) resistors (this study) and only 10^{11} Ω resistors (preliminary tests) indicates that: u_{rel}(signal ratio) is independent of the kind of the used resistor combination. Generally, the relative uncertainties of the signal ratios are smaller for the dissolved crystals (superposition of the laser ablation scattering effect). Blank correction has no significant influence and for the ratios ^{30}Si/^{29}Si u_{rel} decreases by one order of magnitude. An overview of relative uncertainties associated with the signal intensity ratios ^{29}Si/^{28}Si, ^{30}Si/^{28}Si and ^{30}Si/^{29}Si for laser ablation and dissolved samples (table and graphs) is given in the ESI 2† (resistor comparison).

As mentioned in Section 2.2, τ-corrections were applied throughout the measurements using the respective τ-constants of the 10^{13} Ω resistors. To compare influences, sequence 7 of the isotope ratio measurements was measured without the use of τ-correction. No significant change in any final data/results was observed when omitting τ-correction. The direct influence of τ-correction should be observable in the LA measurements: average relative uncertainties of measured intensity ratios (ESI 2†): sequence 7 (without τ-correction): $u_{rel}(^{29}$Si/^{28}Si$) = 0.18\%$, $u_{rel}(^{30}$Si/^{28}Si$) = 0.16\%$, $u_{rel}(^{30}$Si/^{29}Si$) = 0.023\%$. When using τ-correction (e.g. sequence 2: $u_{rel}(^{29}$Si/^{28}Si$) = 0.26\%$, $u_{rel}(^{30}$Si/^{28}Si$) = 0.25\%$, $u_{rel}(^{30}$Si/^{29}Si$) = 0.024\%$) no significant and/or systematic impact/difference can be observed. The dominating impact on the respective uncertainties results from scattering effects of the laser ablation itself: in the current protocol line scans were used which might filter differences in uncertainties of signal ratios. Another explanation of the similar impact of applying/or not τ-correction might be the use of a ns-laser as in our case which favours melting and scattering.

For signal intensity smoothing during LA of WASO04, it was tested first whether a standard polyethylene PE tube ("short" single tube, length 2 m) or better a signal smoothing device ("SQUID") yields a reduced scattering of the data. Fig. 4 displays the raw signals $U(^{28}$Si$)$ of 50 cycles/block on a WASO04 sample of three runs, each comparing the scattering behaviour of a short single tube and a "SQUID".

While the relative standard deviations of the mean in the case of the short single tube range from 1.8% to 2.3%, in the case of the "SQUID", they range only from 1.2% to 1.3%.

For the ratios $U(^{29}$Si$)/U(^{28}$Si$)$ (Fig. 5), the relative standard deviations of the mean in the case of the short single tube range from 0.27% to 0.40%, and when using the "SQUID" from 0.41% to 0.45%. The courses of the signals $U(^{29}$Si$)$ and $U(^{30}$Si$)$ and the ratios yielded similar statistical behaviour with respect to the
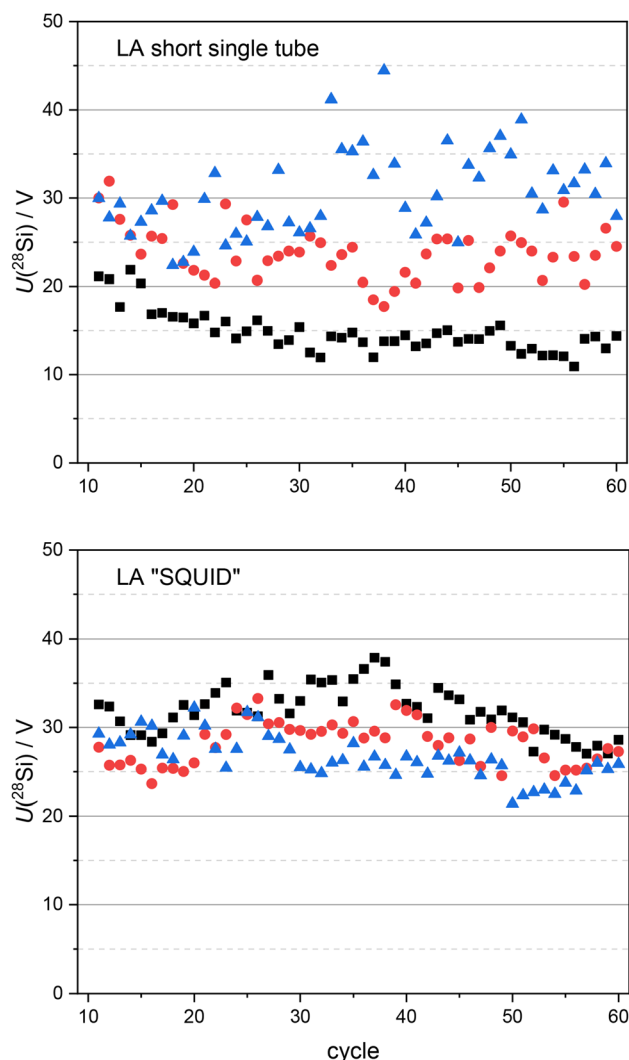

Fig. 4 Upper diagram: ^{28}Si laser ablation signals during 50 cycles of one block (1st run: black squares, 2nd run: red circles, 3rd run: blue triangles) using a common "short" single tube (PE). The lower diagram shows the same for the "SQUID". Laser parameters: rep. rate: 20 Hz, output energy: 50%, scan speed: 6 μm s^{-1}, spot size 40 μm, He flow: 450 mL min^{-1}.

tubing and are not shown here. All corresponding (raw) data and measurements can be found in ESI 1.†

In this study it was decided to use the "SQUID" tube for the laser ablation measurements. The "SQUID" smoothens the original signals by spreading the pulse of the transported ablation aerosol (particle size equilibration).

Another technical problem was observed when using the standard sample positioning device made of plastic inside the two-volume chamber. A larger background (interferences) in the high-mass vicinity of each Si isotope always occurred due to outgassing. After removing most plastic devices from the inner region of the two-volume cell, no relevant background was observed any longer. For a proper positioning of the sample, a home-built aluminum plate covering the total x–y area, adjustable in the z-direction (towards the lens system of the laser) was inserted in the larger area of the two-volume cell (see
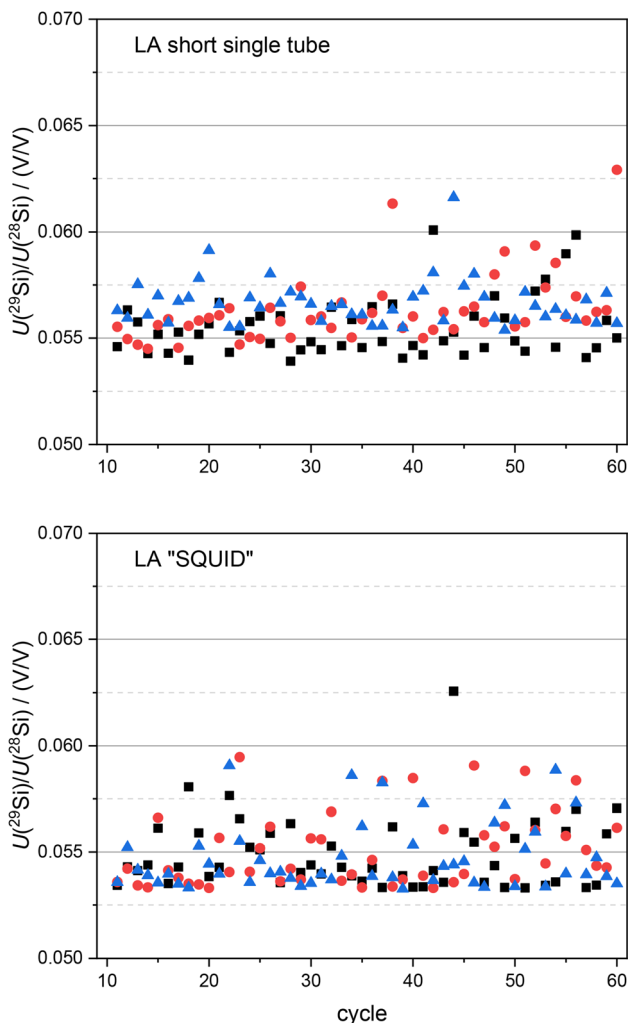
1328 | J. Anal. At. Spectrom., 2025, 40, 1323–1334

This journal is © The Royal Society of Chemistry 2025

Fig. 5 Upper diagram: laser ablation ratios $U(^{29}Si)/U(^{28}Si)$ – not blank corrected – during 50 cycles of one block (1st run: black squares, 2nd run: red circles, 3rd run: blue triangles) using a common "short" single tube (PE). The lower diagram shows the same for the "SQUID". Laser parameters: rep. rate: 20 Hz, output energy: 50%, scan speed: 6 μm s^{-1}, spot size 40 μm, He flow: 450 mL min^{-1}.

"two vol cell" in ESI 1†). This induces background reduction and smoothening of the gas flow due to a highly reduced volume of the incoming He gas flow. A deeper discussion of the sophisticated arrangement of rapid response cells can be found in the literature.[33] Additionally, the He gas flow rate, the laser spot size, and the scan speed were investigated in more detail similarly. The data can be found in the ESI 1.† Finally, the parameters given in Table 2 were applied for the best balance between signal intensity, stability and scattering.

3.2 Calibration factor dependence of dissolved and solid (LA) samples

The determination of isotope ratios using ICP-MS is always accompanied by processes called isotopic fractionation or simply "mass bias". The measured intensity ratios of isotopes differ from the "real" isotope ratios by up to several percent. This has to be corrected by using correction or K factors and has

been a topic of intense research over the past decades.[13,34] Often, certified reference materials – if available – are used to correct for the fractionation effect. When combining solution MC-ICP-MS and laser ablation, mass fractionation is even more complex: the laser ablation process depends on numerous parameters (*e.g.*, kind of transport gas, mass flow, wavelength, frequency, pulse duration and more) as well as on the kind of matrix, the solid sample consists of.[19,20] This will often lead to a large spread of the generated particle sizes transported to the plasma torch. In parallel, the ICP-process itself (plasma conditions) will cause fractionation, too. Often, it is not possible to distinguish between the sources of fractionation due to complex physical processes. The main origins of fractionation of LA-MC-ICP-MS are matrix effects, inhomogeneous particle size distribution (non-uniform aerosol formation), interferences, temperature effects due to laser impact on the sample (different vaporization and condensation, *etc.*).[19,20,35,36]

Isotope ratios traceable to the international system of units (SI) can be obtained applying an absolute method: the measurement of isotope ratios in gravimetric isotope mixtures completely traceable to the SI.[13] The prototype of this procedure has been developed and applied in the context of the XRCD method for the absolute determination of the molar mass of silicon, which is described in detail elsewhere.[11,37] During the measurements, the isotope ratios of a kind of "reference" material have been determined absolutely with associated uncertainties. In the Si case, this material is the WASO04 single crystal with an almost natural isotopic composition.[6,9] When measuring intensity ratios of an unknown Si sample and of the WASO04 material together, a K factor of a certain ratio can be derived as the "true" ratio divided by the measured ratio. The characterization of the "true" isotope ratios of the WASO04 material was applied to the solution (based on TMAH$_{aq}$ as a solvent).[10]

In the near future, WASO04 crystal samples can be used as a solid reference material to analyze Si samples using LA-MC-ICP-MS. Here, it was investigated if and how the K factors derived from the dissolved and the solid material (WASO04) differ and which processes might have an influence. Fig. 6 displays K factors for the correction of the measured intensity ratios (a) $U(^{29}Si)/U(^{28}Si)$, (b) $U(^{30}Si)/U(^{28}Si)$, and (c) $U(^{30}Si)/U(^{29}Si)$ after the measurement of 10 sequences described in Section 2.2.

The underlying raw data and calculations, as well as the reference data of the WASO04 crystal material, are given in the ESI 2.† Two main outcomes are evident: first, the distribution of K factors of the sample in solution (sln) is more unique with lower relative standard deviations of the mean s_{rel} compared to the distribution of K factors determined *via* LA of the solid: $s_{rel}(K_{sln,29/28}) = 0.0088\%$, $s_{rel}(K_{sln,30/28}) = 0.016\%$, and $s_{rel}(K_{sln,30/29}) = 0.0093\%$ in contrast to the solid: $s_{rel}(K_{LA,29/28}) = 0.087\%$, $s_{rel}(K_{LA,30/28}) = 0.097\%$, and $s_{rel}(K_{LA,30/29}) = 0.012\%$. Second, both K factors determined *via* dissolved and solid samples agree well within the limits of uncertainties. The latter clearly approves the application of solid WASO04 material for K factor determination using LA. The larger scattering of single data in the case of LA was caused by a larger distribution of particle sizes as a result of the wavelength (213 nm), which might generate a less complete vaporization than smaller
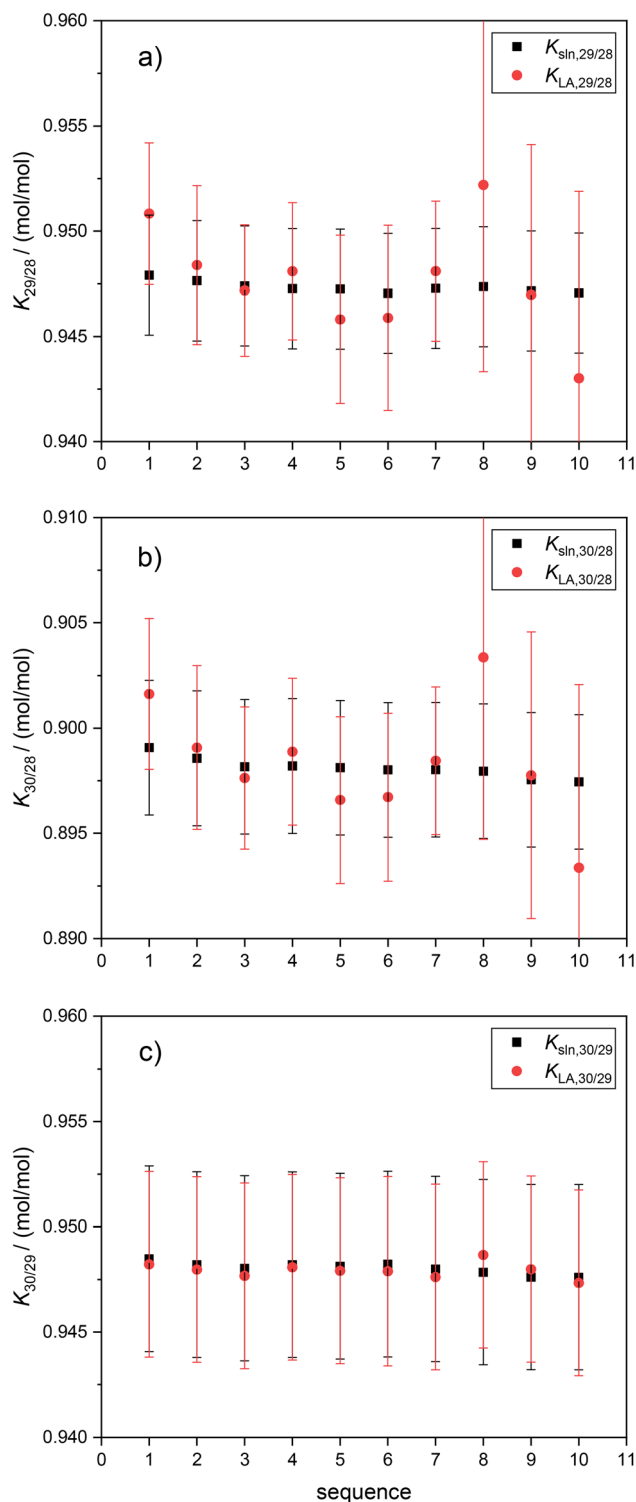
This journal is © The Royal Society of Chemistry 2025

J. Anal. At. Spectrom., 2025, **40**, 1323–1334 | **1329**

Fig. 6 K factors determined from the dissolved (sln, black squares) and the solid samples (red circles) of WASO04 for the correction of the measured intensity ratios: (a) $U(^{29}Si)/U(^{28}Si)$, (b) $U(^{30}Si)/U(^{28}Si)$, and (c) $U(^{30}Si)/U(^{29}Si)$. Error bars denote combined uncertainties ($k = 1$).

wavelengths.[38–40] The same reason can be found in the pulse length (ns), which initiates a prolonged melting after the laser pulse impact compared to state-of-the art fs laser systems.[28] Moreover, the inherent homogeneity of a dissolved sample is

much better than in a solid (surface condition). The applied line scan itself averaging multiple ablation spots, however, will yield a comparable result for the distribution and uncertainties associated with the K factors. Table 3 shows three typical uncertainty budgets of the K factors $K_{29/28}$, $K_{30/28}$, and $K_{30/29}$, with the respective impact quantities derived from dissolved and solid samples. Uncertainty budgets were calculated applying the GUM Workbench Pro™ software (version 2.4.1.392; Metrodata GmbH, Germany) according to the rules of the GUM using the reference values $R(^{29}Si/^{28}Si)$, $R(^{30}Si/^{28}Si)$, and $R(^{29}Si/^{30}Si)$ and the respective amount-of-substance fractions $x(^iSi)$.[9,23] For $K_{29/28}$ (Table 3a) the uncertainty of $x(^{29}Si)$ dominates the uncertainty contributions of the sample in solution by 99.2%. In contrast, the main contributions in the case of the solid sample are the measured intensity ratio $r_{29/28}$ (58.2%) and $x(^{29}Si)$ with 41.5%. A similar distribution of uncertainty components can be observed for $K_{30/28}$ (Table 3b) with a contribution of 99.4% of $x(^{30}Si)$ (dissolved sample) and $r_{30/28}$ (36%) and $x(^{30}Si)$ with 63.7% (solid sample). The uncertainty components of $K_{30/29}$ (Table 3c) show very similar distributions between the dissolved and solid samples.

Due to the large uncertainty contributions of $x(^{29}Si)$ and $x(^{30}Si)$ in case of the ratios $x(^{29}Si)/x(^{28}Si)$ and $x(^{30}Si)/x(^{28}Si)$ it might be reasonable to characterize the amount-of-substance fractions in a future study again. However, for regular molar mass investigations of enriched silicon, they are fit-for-purpose to end up in a lower 10^{-9} range of $u_{rel}(M)$.

3.3   Homogeneity of the solid sample probed by scanning LA

The application of spatially (x- and y-direction) resolved LA enables the investigation of the distribution of sample properties, $e.g.$, chemical purity, surface conditions, isotopic composition, $etc.$ In the case of Si samples used for the XRCD method, in the past, homogeneity studies have been carried out using large cubes (each with a nominal mass of approximately 500 mg) throughout a large single crystal ingot (≈ 50 cm length, ≈ 10 cm diameter) which have been investigated via MC-ICP-MS of dissolved samples. Compared to these relatively large samples and, therefore, somewhat rough studies concerning local distributions of amount-of-substance fractions $x(^iSi)$ of the various isotopes, an LA study yields, in either case, more locally selected results. Since in the current study, scanning LA investigations were executed, we determined the local variations of $x(^iSi)$ on a – for LA – comparable larger area ("quasi-homogeneity") with $\Delta x \approx 5000$ μm $\times$ $\Delta y \approx 1000$ μm. Fig. 1 shows the ten scanning traces (areas) on the sample surface. The total sample has an area of ≈ 225 mm². For each scanning trace, averaged $x(^iSi)$ were evaluated, using the K factors determined from the dissolved reference sample of the respective sequence combining the solid and dissolved sample (using blank corrected intensity ratios of the solid). The raw data and calculations are given in the ESI 2.† Fig. 7 displays the distribution of the $x(^iSi)$ over the ten scanning areas (sequences).

For all three isotopes, the $x(^iSi)$ agree very well within the limits of uncertainty showing at a first glance, that within the averaged scanning areas 1–10, the isotopic distribution is

1330 | J. Anal. At. Spectrom., 2025, 40, 1323–1334

This journal is © The Royal Society of Chemistry 2025

Table 3 Uncertainty budgets of K factors (solution (dissolved) vs. solid)

(a) K factor ($x(^{29}\text{Si})/x(^{28}\text{Si})$: solution vs. solid (LA))

	Quantity	Unit	Best estimate (value)	Standard uncertainty	Sensitivity coefficient	Index, sln	Index, solid
	X_i	$[X_i]$	x_i	$u(x_i)$	c_i	%	%
	$R(^{29}\text{Si}/^{28}\text{Si})$	mol mol^{-1}	0.050700	152×10^{-6}			
Solution	$x(^{29}\text{Si})$	mol mol^{-1}	0.046760	140×10^{-6}	20	99.2	
Solid							41.5
Solution	$x(^{28}\text{Si})$	mol mol^{-1}	0.922280	230×10^{-6}	−1.0	0.7	
Solid							0.3
Solution	$r_{29/28}$	V V^{-1}	0.05354000	5.20×10^{-6}	−18	0.1	
Solid			0.053600	190×10^{-6}			58.2
	Y	$[Y]$	y	$u_c(y)$			
Solution	$K_{29/28}$	mol mol^{-1}	0.94696	2.85×10^{-3}			
Solid			0.94590	4.40×10^{-3}			

(b) K factor ($x(^{30}\text{Si})/x(^{28}\text{Si})$: solution vs. solid (LA))

	Quantity	Unit	Best estimate (value)	Standard uncertainty	Sensitivity coefficient	Index, sln	Index, solid
	X_i	$[X_i]$	x_i	$u(x_i)$	c_i	%	%
	$R(^{30}\text{Si}/^{28}\text{Si})$	mol mol^{-1}	0.033569	120×10^{-6}			
Solution	$x(^{30}\text{Si})$	mol mol^{-1}	0.030960	110×10^{-6}	29	99.4	
Solid							63.7
Solution	$x(^{28}\text{Si})$	mol mol^{-1}	0.922280	230×10^{-6}	−0.97	0.5	
Solid							0.3
Solution	$r_{30/28}$	V V^{-1}	0.03738000	3.60×10^{-6}	−24	0.0	
Solid			0.037440	100×10^{-6}			36.0
	Y	$[Y]$	y	$u_c(y)$			
Solution	$K_{30/28}$	mol mol^{-1}	0.89805	3.20×10^{-3}			
Solid			0.89661	3.99×10^{-3}			

(c) K factor ($x(^{30}\text{Si})/x(^{29}\text{Si})$: solution vs. solid (LA))

	Quantity	Unit	Best estimate (value)	Standard uncertainty	Sensitivity coefficient	Index, sln	Index, solid
	X_i	$[X_i]$	x_i	$u(x_i)$	c_i	%	%
	$R(^{30}\text{Si}/^{29}\text{Si})$	mol mol^{-1}	0.66210	3.08×10^{-3}			
Solution	$x(^{30}\text{Si})$	mol mol^{-1}	0.030960	110×10^{-6}	31	58.5	
Solid							56.0
Solution	$x(^{29}\text{Si})$	mol mol^{-1}	0.046760	140×10^{-6}	−20	41.5	
Solid							39.8
Solution	$r_{30/29}$	V V^{-1}	0.6983000	30.0×10^{-6}	−1.4	0.0	
Solid			0.698500	683×10^{-6}		4.2	4.2
	Y	$[Y]$	y	$u_c(y)$			
Solution	$K_{30/29}$	mol mol^{-1}	0.94817	4.41×10^{-3}			
Solid			0.94789	4.50×10^{-3}			

homogeneous. This behaviour is proven, when calculating the respective degrees-of-equivalence (d_i) for each sequence (scanning area) according to

$$d_i = x_i(^{28}\text{Si}) - x_{av}(^{28}\text{Si}) \qquad (1)$$

Eqn (1) was also applied for ^{29}Si and ^{30}Si (see Fig. 8). The uncertainties $U(d_i)$ ($k = 2$) associated with d_i (here shown for ^{28}Si) are given by

$$U(d_i) = 2 \times \sqrt{u^2(x_i(^{28}\text{Si})) + u^2(x_{av}(^{28}\text{Si}))}$$

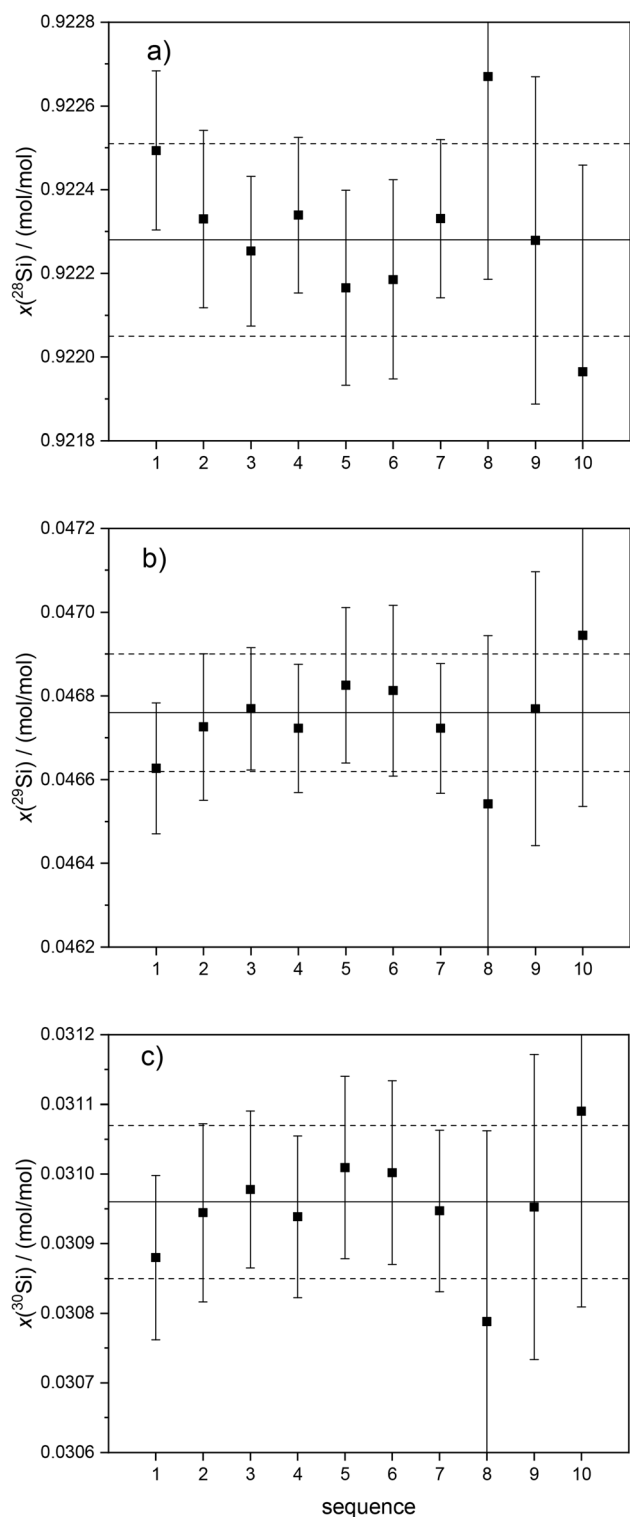$$= 2 \times \sqrt{u^2(x_i(^{28}\text{Si})) + \frac{\sum_{i=1}^{N} u^2(x_i(^{28}\text{Si}))}{N}} \qquad (2)$$

This journal is © The Royal Society of Chemistry 2025

J. Anal. At. Spectrom., 2025, 40, 1323–1334 | 1331

Fig. 7 Amount-of-substance fractions $x(^iSi)$ of the respective Si isotopes ((a) ^{28}Si, (b) ^{29}Si, (c) ^{30}Si) of the solid sample determined during ten sequences (1–10), each representing the scanning areas (1–10) of the WASO04 crystal sample shown in Fig. 1. Error bars denote associated uncertainties ($k = 1$). The solid line shows the arithmetic mean $x_{av}(^iSi)$; dashed lines display upper and lower uncertainties associated with $x_{av}(^iSi)$ with $k = 1$.
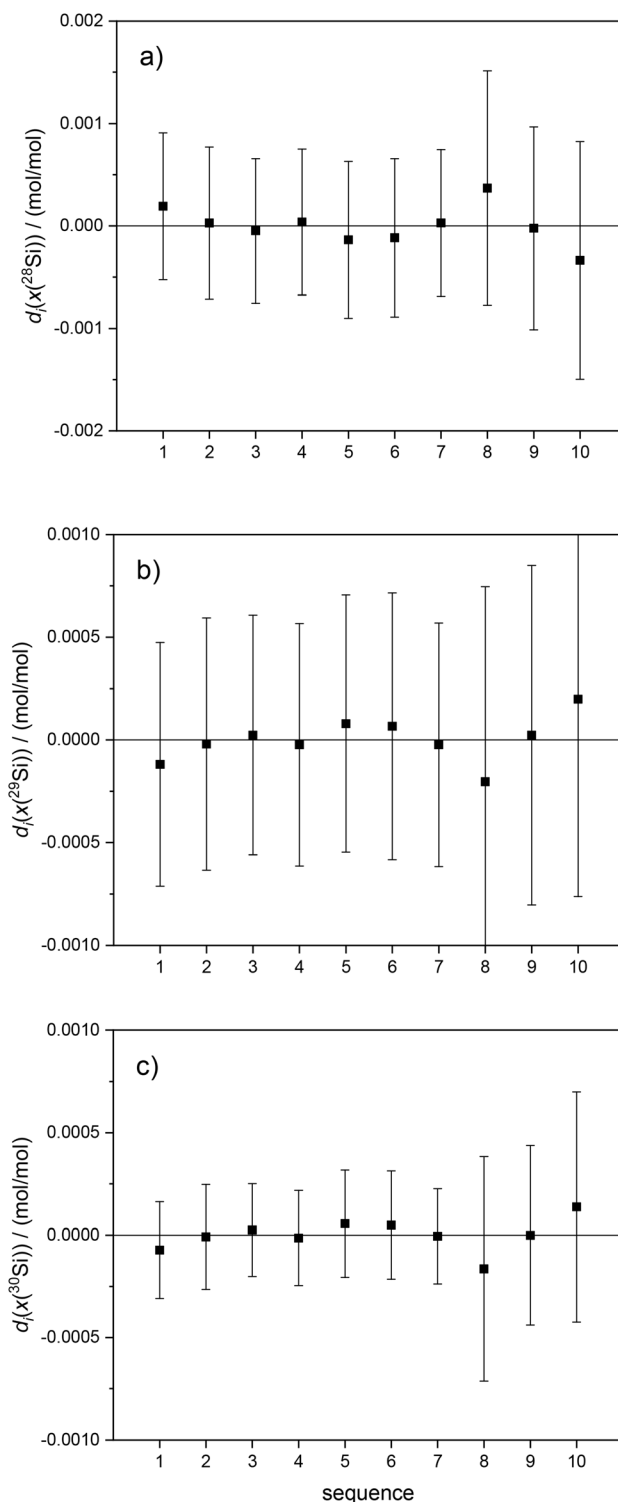
Fig. 8 Degrees of equivalence d_i of amount-of-substance fractions $x(^iSi)$ of the respective Si isotopes ((a) ^{28}Si, (b) ^{29}Si, (c) ^{30}Si) of the solid sample determined during ten sequences (1–10), each representing the scanning areas (1–10) of the WASO04 crystal sample shown in Fig. 1. The expanded uncertainties $U(d_i)$ associated with d_i are displayed as error bars.

1332 | *J. Anal. At. Spectrom.*, 2025, **40**, 1323–1334

This journal is © The Royal Society of Chemistry 2025

This analysis shows clearly that the data sets are consistent (the individual d_i are smaller than their uncertainties) and the error bars encompass the zero line.

This result again proves the ability of the WASO04 crystal material to be a kind of reference material for the *in situ* determination of K factors in the case of pure silicon measurements.

4. Conclusions

Isotope ratio determinations *via* the measurements of intensity ratios can be executed by the combination of dissolved (typical ICP-MS) and solid samples using LA in single measurement sequences. The main challenges in LA are the finding of balanced parameters between signal intensity and fluctuation. Even when operating in the scanning mode (this work), parameters like, *e.g.*, spot size, scan speed, and He gas flow are crucial. An improved protocol for this kind of experiment has been developed and applied for the measurement of isotope ratios of silicon with almost natural isotopic composition (WASO04), which is used as a reference material for the determination of K factors for Si isotope ratios intended for the correction of isotope fractionation (mass bias) *via* the application of gravimetric mixtures. One aim of this study was to compare these K factors determined from the classical sample solution and from laser ablation using the same sample material. In the case of solution measurements, the typical K factors (deviation by a few percent from unity) show relative uncertainties in the range 0.30%–0.46%: $K_{\text{sln}}(x(^{29}\text{Si})/x(^{28}\text{Si})) = 0.94734(28)$ mol mol^{-1}; $K_{\text{sln}}(x(^{30}\text{Si})/x(^{28}\text{Si})) = 0.8981(32)$ mol mol^{-1}; $K_{\text{sln}}(x(^{30}\text{Si})/x(^{29}\text{Si})) = 0.9480(44)$ mol mol^{-1}. K factors derived from LA are in the same range with enlarged relative uncertainties (0.47%–0.60%): $K_{\text{LA}}(x(^{29}\text{Si})/x(^{28}\text{Si})) = 0.9477(50)$ mol mol^{-1}; $K_{\text{LA}}(x(^{30}\text{Si})/x(^{28}\text{Si})) = 0.8983(50)$ mol mol^{-1}; $K_{\text{LA}}(x(^{30}\text{Si})/x(^{29}\text{Si})) = 0.9479(44)$ mol mol^{-1}. Summarized, both K factors derived from the solution as well as from LA measurements agree very well within the limits of uncertainties and show no noticeable matrix dependence. Thus, this very Si sample material (ultrapure single crystalline Si) can be used as a reference material for mass bias correction (K factor determination) in LA studies, yielding the same level of uncertainties as in the case of dissolved samples. The K factor measurements using the solid Si crystal *via* LA serves in parallel as a screening of the homogeneity of the isotopic composition expressed in amount-of-substance fractions $x(^i\text{Si})$ of the respective isotope ^iSi. Ten distinct scanning areas (≈ 5 mm^2) over the Si crystal sample used (total area ≈ 225 mm^2) ensure a representative result. The normalized error E_n for each series ($x(^{28}\text{Si})$, $x(^{29}\text{Si})$, $x(^{30}\text{Si})$) is $\ll 1$, which states that the data are metrologically compatible or equivalent, indicating that the $x(^i\text{Si})$ are chemically/physically homogeneous. In the near future, the improved protocol of this work might be applied to studies concerning isotopic distributions and molar masses as well as respective homogeneity investigations in silicon crystals.

Data availability

The data supporting this article are in the ESI 1 and ESI 2.†

Conflicts of interest

There are no conflicts of interest to declare.

References

1 S. Kainth, P. Sharma, P. K. Diwan and O. P. Pandey, Shaping the Future: Innovations in Silicon Wafer Production and Finishing, *Silicon*, 2024, **16**, 6479–6497.

2 K. Y. Kamal, The Silicon Age: Trends in Semiconductor Devices Industry, *J. Eng. Sci. Technol. Rev.*, 2022, **15**, 110–115.

3 K. Fujii, H. Bettin, P. Becker, E. Massa, O. Rienitz, A. Pramann, A. Nicolaus, N. Kuramoto, I. Busch and M. Borys, Realization of the kilogram by the XRCD method, *Metrologia*, 2016, **53**, A19–A45.

4 G. Bartl, et al., A new ^{28}Si single crystal: counting the atoms for the new kilogram definition, *Metrologia*, 2017, **54**, 693–715.

5 B. Güttler, O. Rienitz and A. Pramann, The Avogadro constant for the definition and realization of the mole, *Ann. Phys.*, 2018, 1800292.

6 P. Becker, H. Bettin, H.-U. Danzebrink, M. Gläser, U. Kuetgens, A. Nicolaus, D. Schiel, P. De Bièvre, S. Valkiers and P. Taylor, Determination of the Avogadro constant via the silicon route, *Metrologia*, 2003, **40**, 271–287.

7 K. Fujii, A. Waseda, N. Kuramoto, S. Mizushima, P. Becker, H. Bettin, A. Nicolaus, U. Kuetgens, S. Valkiers, P. Taylor, P. De Bièvre, G. Mana, E. Massa, R. Matyi, E. G. Kessler Jr and M. Hanke, Present State of the Avogadro Constant Determination from Silicon Crystals with Natural Isotopic Compositions, *IEEE Trans. Instrum. Meas.*, 2005, **54**(2), 854–859.

8 E. G. Kessler, C. I. Szabo, J. P. Cline, A. Henins, L. T. Hudson, M. H. Mendenhall and M. D. Vaudin, The Lattice Spacing Variability of Intrinsic Float-Zone Silicon, *J. Res. Natl. Inst. Stand. Technol.*, 2017, **122**, 1–25.

9 G. D'Agostino, M. Di Luzio, G. Mana, M. Oddone, A. Pramann and M. Prata, ^{30}Si Mole Fraction of a Silicon Material Highly Enriched in ^{28}Si Determined by Instrumental Neutron Activation Analysis, *Anal. Chem.*, 2015, **87**, 5716–5722.

10 A. Pramann, K.-S. Lee, J. Noordmann and O. Rienitz, Probing the homogeneity of the isotopic composition and molar mass of the "Avogadro"-crystal, *Metrologia*, 2015, **52**, 800–810.

11 O. Rienitz, A. Pramann and D. Schiel, Novel concept for the mass spectrometric determination of absolute isotopic abundances with improved measurement uncertainty: part 1 – theoretical derivation and feasibility study, *Int. J. Mass Spectrom.*, 2010, **289**, 47–53.

This journal is © The Royal Society of Chemistry 2025

J. Anal. At. Spectrom., 2025, **40**, 1323–1334 | 1333

12 G. Mana and O. Rienitz, The calibration of Si isotope-ratio measurements, *Int. J. Mass Spectrom.*, 2010, **291**, 55–60.

13 L. Yang, S. Tong, L. Zhou, Z. Hu, Z. Mester and J. Meija, A critical review on isotopic fractionation correction methods for accurate isotope amount ratio measurements by MC-ICP-MS, *J. Anal. At. Spectrom.*, 2018, **33**, 1849–1861.

14 D. Knopf, T. Wiedenhöfer, K. Lehrmann and F. Härtig, A quantum of action on a scale? Dissemination of the quantum based kilogram, *Metrologia*, 2019, **56**, 024003.

15 M. Sargent, H. Goenaga-Infante, K. Inagaki, L. Ma, J. Meija, A. Pramann, O. Rienitz, R. Sturgeon, J. Vogl, J. Wang and L. Yang, The role of ICP-MS in inorganic chemical metrology, *Metrologia*, 2019, **56**, 034005.

16 D. Günther, S. E. Jackson and H. P. Longerich, Laser ablation and arc/spark solid sample introduction into inductively coupled plasma mass spectrometers, *Spectrochim. Acta, Part B*, 1999, **54**, 381.

17 R. E. Russo, X. Mao, J. J. Gonzalez, V. Zorba and J. Yoo, Laser Ablation in Analytical Chemistry, *Anal. Chem.*, 2013, **85**, 6162.

18 A. L. Gray, Solid Sample Introduction by Laser Ablation for Inductively Coupled Plasma Source Mass Spectrometry, *Analyst*, 1985, **110**, 551–556.

19 W. Zhang and Z. Hu, A critical review of isotopic fractionation and interference correction methods for isotope ratio measurements by laser ablation multi-collector inductively coupled plasma mass spectrometry, *Spectrochim. Acta, Part B*, 2020, **171**, 105929.

20 Matrix Effects in Laser Ablation-ICP-MS, in *Laser Ablation ICP-MS in the Earth Sciences*, ed. P. S. Sylvester, 2008, vol. 40.

21 J. M. Koornneef, C. Bouman, J. B. Schwieters and G. R. Davies, Measurement of small ion beams by thermal ionisation mass spectrometry using new 10^{13} Ohm resistors, *Anal. Chim. Acta*, 2014, **819**, 49–55.

22 A. Pramann and O. Rienitz, Comparison and influence of 10^{11} and 10^{13} ohm resistors used for MC-ICP-MS determination of isotope ratios in highly enriched silicon, *J. Anal. At. Spectrom.*, 2024, **39**, 1540–1550.

23 BIPM, IEC, IFCC, ILAC, ISO, IUPAC, IUPAP and OIML, *Evaluation of measurement data − guide to the expression of uncertainty in measurement*, 2008, JCGM 100:2008.

24 A. Pramann and O. Rienitz, The isotopic composition of the new enriched silicon crystal Si28-31Pr11: maintaining the realization and dissemination of the mole and the kilogram via the XRCD method, *Metrologia*, 2024, **61**, 025005.

25 G. Craig, Z. Hu, A. Zhang, N. S. Lloyd, C. Bouwman and J. Schwieters, *Dynamic time correction for high precision isotope ratio measurements*, Technical Note 30396, Thermo Fisher Scientific Inc., 2019.

26 A. Gourgiotis, G. Manhès, P. Louvat, J. Moureau and J. Gaillardet, Transient signal isotope analysis using multicollection of ion beams with Faraday cups equipped with 10^{12} Ω and 10^{11} Ω feedback resistors, *J. Anal. At. Spectrom.*, 2015, **30**, 1582–1589.

27 L. Michaliszyn, Beiträge zur Ermittlung der Reinheit von natürlichem hochreinen Silicium mit Hilfe der Kopplung von Laser-Ablation und hochauflösender ICP-MS, *Doctoral dissertation*, Universität Leipzig, 2023, DOI: 10.7795/110.20231208.

28 J. Chmeleff, I. Horn, G. Steinhoefel and F. von Blanckenburg, In situ determination of precise stable Si isotope ratios by UV-femtosecond laser ablation high-resolution multi-collector ICP-MS, *Chem. Geol.*, 2008, **249**, 155–166.

29 M. Holá, Z. Salajková, F. Gregar, J. Ondráček, D. Pavlinák, P. Šperka, A. Hrdlička, J. Kaiser and V. Kanický, Laser spot overlap in scanning laser ablation ICP-MS analysis: impact on analytical signal and properties of the generated aerosol, *Spectrochim. Acta, Part B*, 2024, **219**, 106999.

30 A. Tunheng and T. Hirata, Development of signal smoothing device for precise elemental analysis using laser ablation-ICP-mass spectrometry, *J. Anal. At. Spectrom.*, 2004, **19**, 932–934.

31 Y. Kon, T. D. Yokoyama and M. Ohata, Analytical Efficacy of a Gas Mixer and Stabilizer for Laser Ablation ICP Mass Spectrometry, *ACS Omega*, 2020, **5**, 28073–28079.

32 M. Susset, A. Leduc-Gauthier, A.-C. Humbert, F. Pointurier and C. Pécheyran, Comparison of the fluctuations of the signals measured by ICP-MS after laser ablation of powdered geological materials prepared by four methods, *Anal. Sci.*, 2023, **39**, 999–1014.

33 S. J. M. Van Malderen, A. J. Managh, B. L. Sharp and F. Vanhaecke, Recent developments in the design of rapid response cells for laser ablation-inductively coupled plasma-mass spectrometry and their impact on bioimaging applications, *J. Anal. At. Spectrom.*, 2016, **31**, 423–439.

34 L. Yang, Accurate and Precise Determination of Isotopic Ratios by MC-ICP-MS: A Review, *Mass Spectrom. Rev.*, 2009, **28**, 990–1011.

35 J. Košler, H. P. Longerich and M. N. Tubrett, Effect of oxygen on laser-induced elemental fractionation in LA-ICP-MS analysis, *Anal. Bioanal. Chem.*, 2002, **374**, 251–254.

36 J. Míková, J. Košler, H. P. Longerich, M. Wiedenbeck and J. M. Hanchar, Fractionation of alkali elements during laser ablation ICP-MS analysis of silicate geological samples, *J. Anal. At. Spectrom.*, 2009, **24**, 1244–1252.

37 A. Pramann, O. Rienitz, D. Schiel, B. Güttler and S. Valkiers, Novel concept for the mass spectrometric determination of absolute isotopic abundances with improved measurement uncertainty: part 3—molar mass of silicon highly enriched in ^{28}Si, *Int. J. Mass Spectrom.*, 2011, **305**, 58–68.

38 *Laser Ablation*, ed. J. C. Miller, Springer Series in Material Science 28, Springer, Berlin, 1994.

39 M. Raj Marks, K. Yew Cheong and Z. Hassan, A review of laser ablation and dicing of Si wafers, *Precis. Eng.*, 2022, **73**, 377–408.

40 C. Zhang, H. Zhao, W. Zhang, T. Luo, M. Li, K. Zong, Y. Liu and Z. Hu, A high performance method for the accurate and precise determination of silicon isotopic compositions in bulk silicate rock samples using laser ablation MC-ICP-MS, *J. Anal. At. Spectrom.*, 2020, **35**, 1887–1896.

1334 | *J. Anal. At. Spectrom.*, 2025, **40**, 1323–1334

This journal is © The Royal Society of Chemistry 2025